ADVANCES IN ATMOSPHERIC SCIENCES, VOL. 22, NO. 2, 2005, 246–259

Study of Initial Vorticity Forcing for Block Onset by a 4-Dimensional Variational Approach

QIAO Fangli*[1] (乔方利), ZHANG Shaoqing[2] (张绍晴), and YIN Xunqiang[1] (尹训强)

[1] *First Institute of Oceanography, State Oceanic Administration, Qingdao* 266061

[2] *Geophysical Fluid Dynamics Laboratory, Princeton University, Princeton, NJ* 08542, *USA*

(Received 11 February 2004; revised 25 September 2004)

ABSTRACT

With the aid of a global barotropic model, the role of the interaction of the synoptic-scale disturbance and the planetary flow in block onset is examined by a 4-dimensional variational approach. A cost function is defined to measure the squared errors of the forecasted stream functions during block onset period (day 4 and day 5 in this study) over a selected blocking domain. The sensitivity of block onset with respect to the initial synoptic-scale disturbance is studied by examining the gradient of the defined cost function with respect to the initial (during the first 24 hours) vorticity forcing, which is evaluated by the adjoint integration. Furthermore, the calculated cost function and gradient are connected with the limited-memory quasi-Newton optimization algorithm for solving the optimal initial vorticity forcing for block onset. For two studied cases of block onset (northern Atlantic and northern Pacific) introducing the optimal initial vorticity forcing, the nonlinear barotropic advection process mostly reconstructs these blocking onset processes. The results show that the formation of blocking can be correctly described by a barotropic nonlinear advection process, in which the wave- (synoptic-scale) flow (planetary-scale) interaction plays a very important role. On an appropriate planetary-scale flow, a certain synoptic-scale disturbance can cause the blocking onset by the interaction between the synoptic scale perturbations and the planetary scale basic flows. The extended forecasts show that the introduction of the optimal initial vorticity forcing can predict the blocking process up to the 7th or 8th day in this simple model case. The experimental results in this study show that the 4-dimensional variational approach has a good potential to be applied to study the dynamics of the medium-range weather processes. This simple model case study is only an initial trial. Applying the framework in this study to a complex model will further our understanding of the mechanism of the atmospheric/oceanic processes and improve their prediction.

Key words: 4D variation, block onset, global barotropic model

1. Introduction

Blocking is a persistent anomaly of the large-scale circulation of the atmosphere at middle and high latitudes (Rex, 1950; Dole and Gordon, 1983). The dynamics of the anomaly circulation have been a hot topic of considerable scientific interest since, during blocking, the local weather often exhibits extremes. There are many theories that try to understand the mechanism of blocking: multiple flow equilibrium (Charney and DeVore, 1979), instability (Frederiksen, 1982), resonance mode (Tung and Lindzen, 1979) and low-frequency oscillation (Nakamura and Wallace, 1990), etc. It is well known (Berggren et al., 1949; Namias, 1964; Sanders and Gyakum, 1980; Reinhold and Pierrehumbert, 1982; Shutts, 1983; Tibaldi and Buzzi, 1983; Colucci, 1985; Colucci and Alberta, 1996) that the interaction of synoptic-planetary scales is an important mechanism of the atmospheric blocking.

Efforts (Colucci, 1985, 1987; Dole, 1989; Tsou and Smith, 1990; Lupo and Smith, 1995; Colucci and Alberta, 1996) have been made to find out the relationship between atmospheric blocking and antecedent, upstream cyclone activities for improving the forecast of blocking events. Colucci and Alberta (1996), from statistics on a great number of cases, investigated the preconditioning characteristics of planetary waves. They found that if a lower tropospheric explosive cyclogenesis occurs over a region in which the

*E-mail: qiaofl@fio.org.cn or flqiao@21cn.com

50 KPa geostrophic u, v and their anomalies u' and satisfy $v' > 0, u' < 0$ and $v/u > 0.5$, then the likelihood of block onset exceeds the climatological expection within 5 days and 60° of the explosive cyclogenesis. Identifying fast growth modes as the precursor of blocking anomalies has been the other aspect of the efforts (Frederiksen, 1989; Frederiksen and Bell, 1990; Frederiksen, 1998).

Since optimal control theory was introduced into atmospheric numerical analysis (Le Dimet and Talagrand, 1989), the adjoint of a numerical model has been used to calculate the sensitivity of a model aspect. Zou et al. (1993) applied the adjoint sensitivity formalism of Cacuci (1981a, b) into a two-layer isentropic model to examine the sensitivity of a blocking index to the initial vorticity sources. This technique was expanded to examine the sensitivity of the efficacy of modal and non-modal perturbations in causing block onset (Pondeca et al., 1998). Others (Li et al., 1999) used the derived sensitivity information by adjoint equations to approximate the initial vorticity forcing to study block onset.

This study applies a 4-dimensional variational approach to calculate the optimal initial vorticity forcing for block onset and examines the impact of the derived optimal initial vorticity forcing on blocking simulation and forecast. After a brief description of a global barotropic spectral model and its adjoint in section 2, the relative data and methodology are presented in section 3. The results including the calculated sensitivity distribution using the adjoint equation and the derived optimal initial vorticity forcing by the optimization procedure which combines the nonlinear model, the adjoint and a quasi-Newton minimization algorithm are exhibited in section 4. Section 5 examines the impact of the derived optimal initial vorticity forcing on blocking simulation and forecast. Conclusions and discussions are given in section 6.

2. A global barotropic spectral model and its adjoint

2.1 *A global barotropic spectral (GBS) model*

The fundamental basis of a barotropic model is the barotropic vorticity advection equation. Certain modifications (introduction of the Cressman parameter and the real terrain, for instance) can improve its single level and nondivergency limits. Based on the equation of conservation of potential vorticity (Haltiner and Williams, 1980) with the consideration of the terrain effect, a modified barotropic vorticity equation can be written as

$$\frac{\partial}{\partial t}(\nabla^2 - \lambda^2)\psi + J(\psi, \nabla^2\psi) + \beta\frac{\partial\psi}{\partial x} + J(\psi, h') = f_c \tag{1}$$

where ψ is the geostrophic streamfunction, β is the change rate of the Coriolis parameter with latitude, J is the Jacobian operator, $h' = (f_0/H_0)h_{\text{terrain}}$ represents the effect of topography, h_{terrain} and f_c represents the vorticity forcing. Here

$$\lambda^2 = \frac{f^2}{gH_0}$$

is the Cressman parameter, f the planetary vorticity, and H_0 the average atmospheric "equivalent depth".

When Eq. (1) is expanded on a mesh system over the global domain, the barotropic model can be written in a matrix form as

$$\frac{\partial\psi}{\partial t} = \boldsymbol{F}(\psi, \boldsymbol{f}_c) \tag{2}$$

where $\boldsymbol{F}(\psi, \boldsymbol{f}_c)$ is a matrix notation of all contributions for the time tendency in Eq. (1). In this study, time integration is only for spectral coefficients in which a rhomboidal 21 truncation is applied for the transformation between spectral coefficients and grid values. (For a gridpoint model, solving the Helmholtz equation is involved for each updating time step of the streamfunction ψ). $\boldsymbol{f}_c$ is the vorticity forcing vector. The Gaussian grid includes 54 (lat)×64 (long) gridpoints. Like most numerical models, except that a forward time integration is used for the first time step (stepsize=30 min), a leap-frog time integration scheme is used to forward the model. An Asselin time filter (Asselin, 1972)

$$\psi_1 = \frac{1}{2}\varepsilon\psi_{t-1} + (1-\varepsilon) + \frac{1}{2}\varepsilon\psi_{t+1} \tag{3}$$

is applied for damping spurious computational modes, where ε is the Asselin filter coefficient.

2.2 *The tangent linear model (TLM) and adjoint of the GBS model*

For coding the adjoint of the GBS model, first, we differentiate all nonlinear terms in Eq. (1) to develop TLM. If we restrict the control parameters to be initial conditions of the streamfunction and the vorticity forcing, the TLM that governs the evolution of a perturbed state along the trajectory of the basic state can be written as

$$\frac{\partial}{\partial t}(\nabla^2 - \lambda^2)\delta\psi + J(\delta\psi, \nabla^2\psi) + J(\psi, \nabla^2\delta\psi) + \beta\frac{\partial\delta\psi}{\partial x} + J(\delta\psi, h') = \delta f_c\,, \tag{4}$$

or in matrix form as

$$\frac{\partial\delta\psi}{\partial t} = \boldsymbol{F}'_{\psi}(\psi, \boldsymbol{f}_c)\delta\psi + \boldsymbol{F}'_{\boldsymbol{f}_c}(\psi, \boldsymbol{f}_c)\delta\boldsymbol{f}_c\,, \tag{5}$$

where $\delta(\cdot)$ represents the perturbation and $(\cdot)$ represents the basic state. $\boldsymbol{F}'_{\psi}(\psi,\boldsymbol{f}_{\rm c})$ and $\boldsymbol{F}'_{\boldsymbol{f}_{\rm c}}(\psi,\boldsymbol{f}_{\rm c})$ are respectively the first derivatives of $\boldsymbol{F}(\psi,\boldsymbol{f}_{\rm c})$ with respect to ψ and $\boldsymbol{f}_{\rm c}$. Then we differentiate all nonlinear terms in the GBS model to code the TLM Eq.(5). Next, through the "adjoint of finite difference" approach (Sirkes and Tziperman, 1997), we code adjoints by transposing all DO loops and subroutines in the TLM. If $L = L_n \ldots L_2 L_1$ represents the propagator of the TLM such as $\delta\psi_t = L_n \ldots L_2 L_1 \delta\psi_0$, then a transposed version $L_* = L_{*,1} L_{*,2} \ldots L_{*,n}$ represents its adjoint. When we performed an inner product check such as $\langle L\delta\psi, L\delta\psi\rangle = \langle \delta\psi, L_* L\delta\psi\rangle$, it agreed to 15 decimal places in 64-bit arithmetic when the model was run at rhomboidal 21 truncation with a leap-frog time integration for 120 hours with a 30-minute time step.

3. Data and methodology

3.1 *Two blocking cases*

The streamfunctions in this study are derived using the 50 kPa u and v extracted from ECMWF (European Centre for Medium-Range Weather Forecasts) re-analysis data. Case 1 chosen in this study for block onset is a blocking process that occurred during the end of December 1990 and the beginning of 1991. Figure 1 presents the daily evolution of streamfunctions on 50 kPa isohypses starting from 0000 UTC 28 December 1990. At the end of December 1990, over the east of the North Pacific a high ridge was maintained and over the west of the ridge was a low trough. On 30 December the ridge strengthened and developed to the north. On 31 December an "Ω" pattern blocking onset over the high-latitude regions in the North Pacific, which centered over eastern Siberia and the Bering Strait, covering a region south to the Aleutian Islands and north to the Chukchi Sea. This blocking reached its mature phase on 1 January 1991 and the "Ω" pattern was maintained until 3 January. On 4 January the blocking high degraded to a high ridge and gradually weakened further.

Case 2 chosen for this study is a "dipole" pattern blocking process over the eastern North Atlantic and the west coast of Europe that occurred during early November 1980. As shown in Fig. 2, at the beginning of November 1980, a high ridge developed over western Europe, and over both its downstream and upstream areas, central Europe and the central North Atlantic, were two troughs. With the development of these troughs and ridge, a dipole blocking onset on 5 November 1980 and was maintained until 7 November. Afterward, the cut-off low and blocking high slightly weakened but were maintained by 9 November. After 10 November, the blocking structure further weakened and degraded to a trough and ridge.

3.2 *The cost function measuring the forecast errors over a local domain*

Many investigations have shown that blocking processes have the initial vorticity forcing as preconditions (Shutts, 1983; Colucci and Alberta, 1996; Frederiksen, 1998). The real application of these theoretical or empirical postulates is difficult due to the shortage of quantitive accuracy for the location and the amplitude of the vorticity forcing. In order to solve for the precondition of the blocking process, we inversely retrieve the optimal vorticity forcing using a 4-dimensional variational approach. The cost function is defined as a sum of squared forecasting errors of the streamfunctions during the block onset period over a local domain which is occupied by the blocking. Then the cost function can be expressed as

$$J(\boldsymbol{f}_{\rm c}) = \frac{1}{2}\sum_{t=t_r}^{t_R} (\psi_{{\rm f},D} - \psi_{{\rm a},D})^{\rm T} (\psi_{{\rm f},D} - \psi_{{\rm a},D}) \,, \qquad (6)$$

where $\psi_{{\rm f},D}$ and $\psi_{{\rm a},D}$ represent respectively the modeled and analyzed streamfunction vectors over the local blocking domain, D, as shown by the shaded regions in Fig. 3 in which panel (a) represents Case 1 and panel (b) represents Case 2. (t_r, t_R) is the time window over which the cost function is defined. In this study, the verification time window is set as the last 48 hours of the 5-d forecasts. For example, for Case 1 and Case 2, the cost function represents the sum of squared forecast errors of the streamfunctions from hour 72 to hour 120 starting from 0000 UTC 28 December 1990 and 0000 UTC 1 November 1980, respectively, over domain D. The root mean squares (RMS) of the forecast errors of streamfunctions during the 48-h period are shown in Fig. 3 by thick lines. The time means of the ECMWF re-analysis streamfunctions from 0000 UTC 31 December 1990 to 0000 UTC 2 January 1991 (panel a), from 0000 UTC 4 November 1980 to 0000 UTC 6 November 1980 (panel b), are also plotted in Fig. 3 by thin lines for reference.

$\boldsymbol{f}_c$ in Eq. (6) represents a stationary vorticity forcing vector during some initial period (initial 24 hours in this study). Minimizing $J(\boldsymbol{f}_{\rm c})$ of Eq. (6) by adjusting the initial vorticity forcing vector $\boldsymbol{f}_{\rm c}$ gives us a strong constraint experiment, i.e. under the constraint of the barotropic vorticity advection Eq. (1), we vary the initial vorticity forcing to force the modeled streamfunctions over the local blocking domain close to the re-analysis streamfunctions as much as possible. Through the process we try to understand the importance of the initial vorticity forcing in the formation of blocking processes.

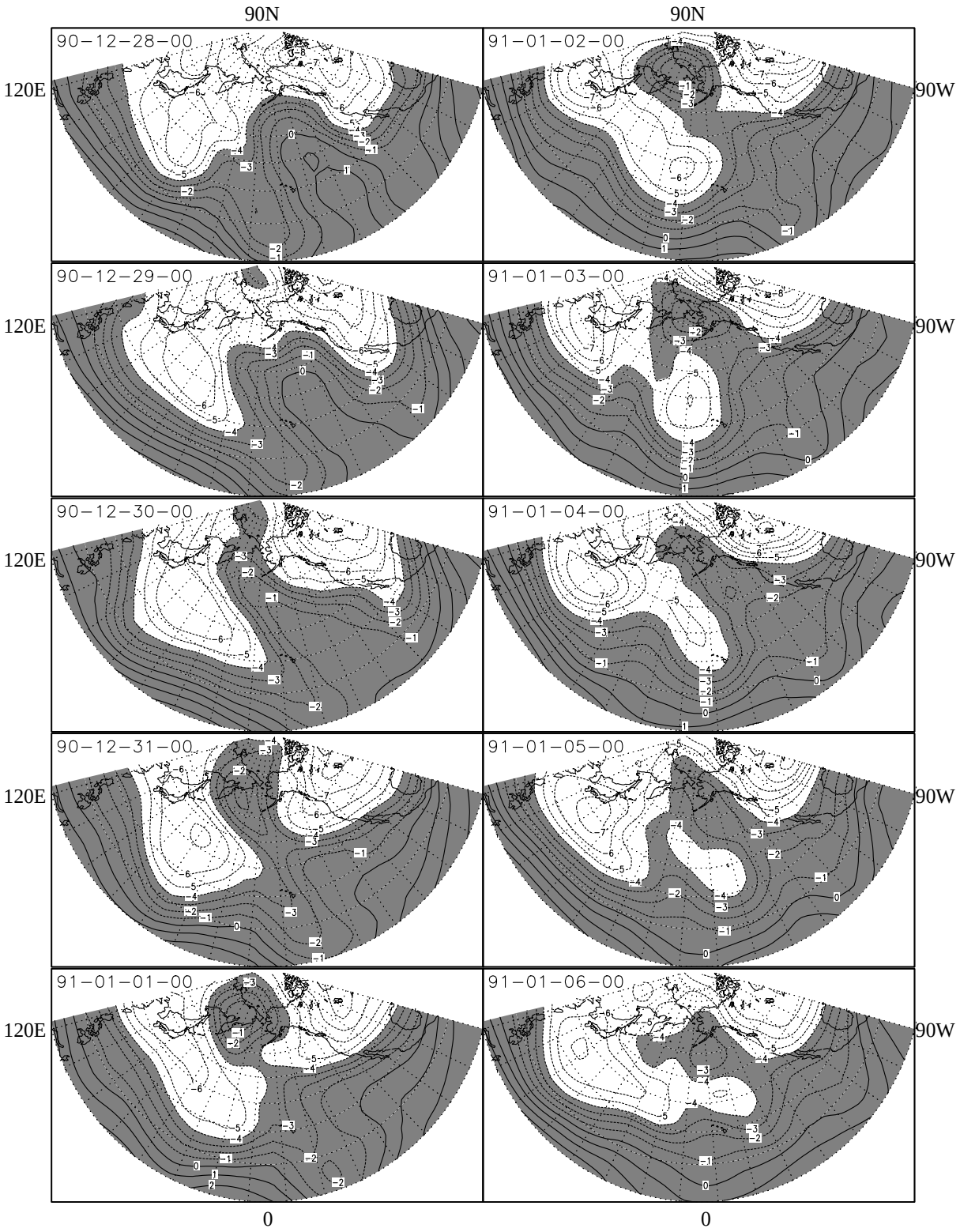

Fig. 1. Daily evolution of the stream function from 0000 UTC 28 December 1990 to 0000 UTC 6 January 1991 over the domain of 0°–90°N, 120°–270°E. The contours are in increments of 10^7 m^2 s^{-1}.

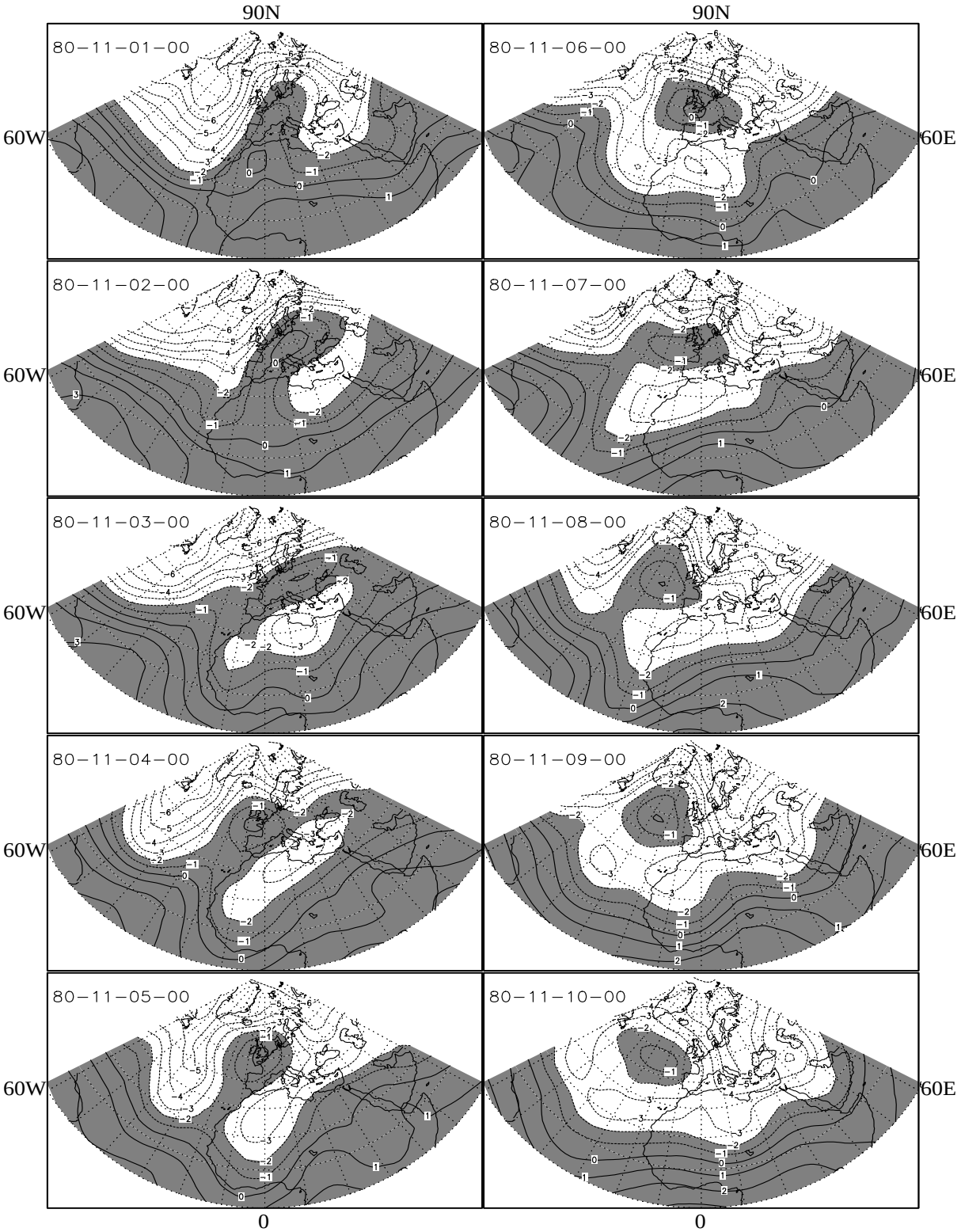

Fig. 2. Same as Fig. 1, except from 0000 UTC 1 November 1980 to 0000 UTC 10 November 1980 over the domain of 0°–90°N, 60°W–60°E.

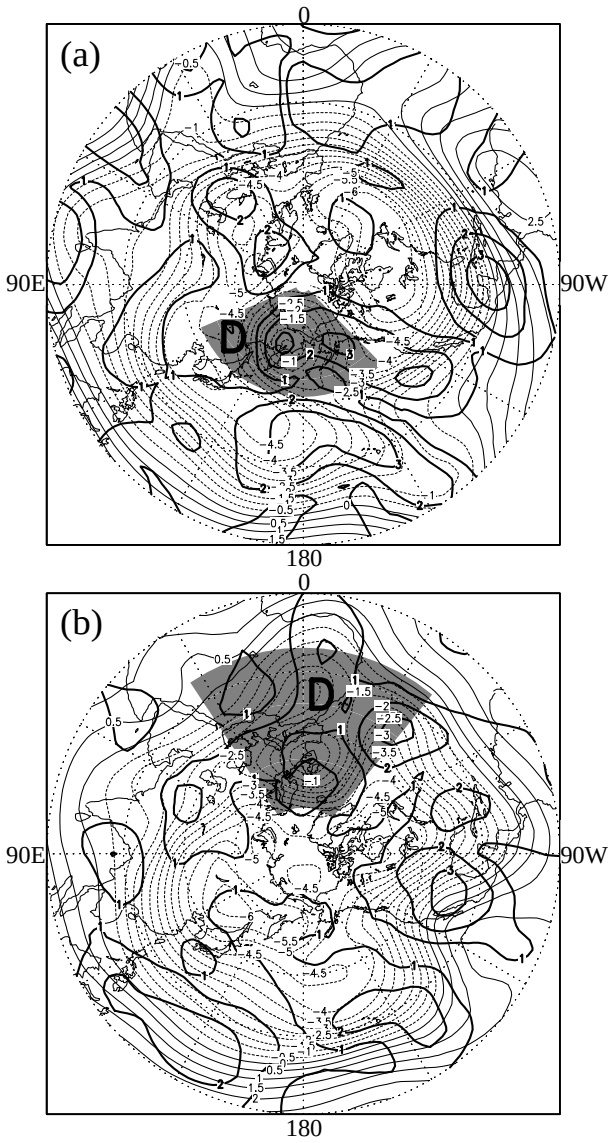

Fig. 3. Distributions of the time mean of forecast errors (thick line) from hour 72 to hour 120 with the initial conditions at (a) 0000 UTC 28 December 1990 and (b) 0000 UTC 1 November 1980 over the Northern Hemisphere. Distributions of the time mean of the analysis streamfunctions (thin line) (a) from 0000 UTC 31 December 1990 to 0000 UTC 2 January 1991 and (b) from 0000 UTC 4 to 0000 UTC 6 November 1980 are plotted as the background. The contours are in increments of 10^6 m^2 s^{-1} (thick lines) and 10^7 m^2 s^{-1} (thin lines). The shaded region marked by the symbol "D" is the selected domain on which the cost function is defined for block onset.

3.3 *Calculation of the gradient of the cost function*

The goal of this study is to find an optimal initial vorticity forcing vector $\boldsymbol{f}_{\text{opt, c}}$ which minimizes the cost function defined by Eq. (6). An adjoint integration backward in time evaluates the gradient of the cost function with respect to the initial vorticity forcing ($\nabla_{\boldsymbol{f}_\text{c}} J$). This process can be symbolically written as

$$\begin{cases} -\dfrac{\partial \delta \hat{\boldsymbol{f}}_\text{c}}{\partial t} - \left(\dfrac{\partial \boldsymbol{F}(\psi, \boldsymbol{f}_\text{c})}{\partial \boldsymbol{f}_\text{c}}\right)^\text{T} \delta \hat{\boldsymbol{f}}_\text{c} = \psi_{\text{f},D} - \psi_{\text{a},D} \\ \nabla_{\boldsymbol{f}_\text{c}} J = \int_{t_R}^{t_0} \delta \hat{\boldsymbol{f}}_\text{c} dt \end{cases} \tag{7}$$

where $\delta \hat{\boldsymbol{f}}_\text{c}$ is the adjoint variable related to the initial vorticity forcing vector $\boldsymbol{f}_\text{c}$. As an application of the chain rule, the adjoint integration efficiently evaluates the gradient of the cost function with respect to control variables although the tangent linear approximation may not validly describe the evolution of a small perturbation (Zhang et al., 2001) for a long forecast leading time. Therefore, we can use the adjoint model to evaluate the gradient of J in Eq. (6) defined by forecasts out of 5 days with respect to the initial vorticity forcing ($\boldsymbol{f}_\text{c}$).

A gradient test is necessary to guarantee that the gradient that calculated from the adjoint integration is correct. From the first order approximation of the Taylor expansion of the cost function, one defines a ratio to measure the consistency between the linear increment along the gradient direction of J and a perturbed J (Navon et al., 1992) as

$$\Phi(\alpha) = \frac{J(\boldsymbol{f}_\text{c} + \alpha \boldsymbol{e}) - J(\boldsymbol{f}_\text{c})}{\alpha \boldsymbol{e}^\text{T} \nabla_{\boldsymbol{f}_\text{c}} J} = 1 + O(\alpha) \tag{8}$$

where α is a small scalar governing the magnitude of perturbations and $\boldsymbol{e}$ is a unit vector such as $\boldsymbol{e} = -\nabla_{\boldsymbol{f}_\text{c}} J \parallel \nabla_{\boldsymbol{f}_\text{c}} J \parallel^{-1} \times 10^{-9}$. Equation (8) shows that when α is small, for a correct gradient $\nabla_{\boldsymbol{f}_\text{c}} J, \Phi(\alpha)$ goes to 1 as α is small but not a machine zero. We choose the period from 0000 UTC 31 December 1990 to 0000 UTC 2 January 1991 as the blocking onset phase and

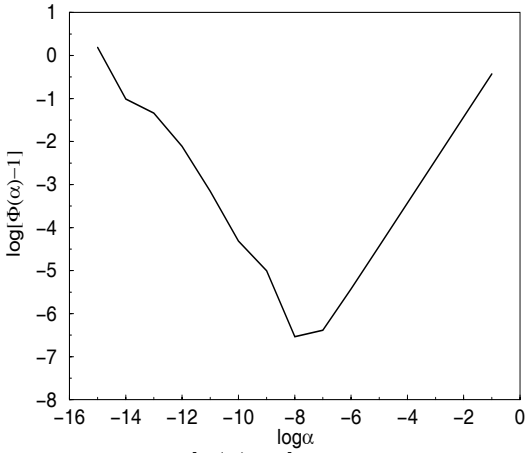

Fig. 4. Change of $\log[\Phi(\alpha) - 1]$ with $\log\alpha$ for the gradient test.

use 0000 UTC 28 December 1990 as the initial condition to carry out the gradient test as Eq. (8) to form Fig. 4, which presents the curve of the logarithm of $\Phi(\alpha) - 1$ with respect to $\log\alpha$. The figure shows that the adjoint integration correctly calculates the gradient of $J(\boldsymbol{f}_c)$ with respect to the initial vorticity forcing vector $\boldsymbol{f}_c$ since a linear increment of J along the derived gradient direction always sufficiently represents the perturbed cost function by $\alpha\boldsymbol{e}$ as $\alpha = 10^{-14}-10^{-1}$.

Now that the gradient of $J(\boldsymbol{f}_c)$ is available, in section 4.2 we will employ a limited memory quasi-Newton algorithm (Liu and Nocedal, 1989) to minimize $J(\boldsymbol{f}_c)$ with respect to $\boldsymbol{f}_c$ so as to solve for the optimal initial vorticity forcing.

4. Numerical results

4.1 *The sensitivity distribution of blocking with respect to the initial vorticity forcing*

Using the analysis streamfunctions at 0000 UTC 28 December 1990 (Case 1) and 0000 UTC 1 November 1980 (Case 2) from the ECMWF re-analysis data as initial conditions, the nonlinear GBS model is first integrated up to 5 days without the vorticity forcing to calculate the J by Eq. (6) using the last 48-h (from hour 72 to hour 120) forecasted sreamfunctions. Then the adjoint model is integrated backward in time by collecting the first derivatives of J with respect to the modeled streamfunction in this 48-hour time window as input. While the time of the integration goes back to the initial time, the adjoint variable $\delta\hat{\boldsymbol{f}}_c$ represents the gradient of J with respect to the initial vorticity forcing, $\boldsymbol{f}_c$, by Eq. (7). If the adjoint variable of $\delta\hat{\boldsymbol{f}}_c$ is accumulated over the initial 24 hours, distributions of the calculated gradient tell us where and how much it is sensitive to the blocking onset if a stationary vorticity forcing is put into the model during the initial 24 hours.

Figure 5a and 5b display the sensitivity distributions of the blocking onset in Case 1 and Case 2 respectively with respect to the initial 24-h vorticity forcing. The time means of the analysis streamfunctions over the 48 hours are plotted as the references for both cases. Both panels show that the negative sensitivity is located over the south and the west of the blocking while positive sensitivity is always located over the blocking region itself and east of the blocking region. Since these sensitivity distributions are derived as the initial vorticity forcing is zero, the positive/negative sensitivity always means a negative/positive vorticity forcing is needed over the corresponding regions. Therefore, these negative/positive sensitivity distributions reflect the positive/negative vorticity demand for the blocking onset. This kind of initial vorticity forcing representing a synoptic scale disturbance can generate and transport the positive/negative vorticity to trigger and maintain the block. From Fig. 5, it is observed that for the "Ω" pattern blocking case (panel a) the strength of positive/negative sensitivity is almost even while for the "dipole" pattern blocking case (panel b) the strength of positive sensitivity is much less than that of negative sensitivity. This means that to form the "dipole" blocking, the development of a trough to the southwest of the blocking is much more important than the strengthening of the ridge itself.

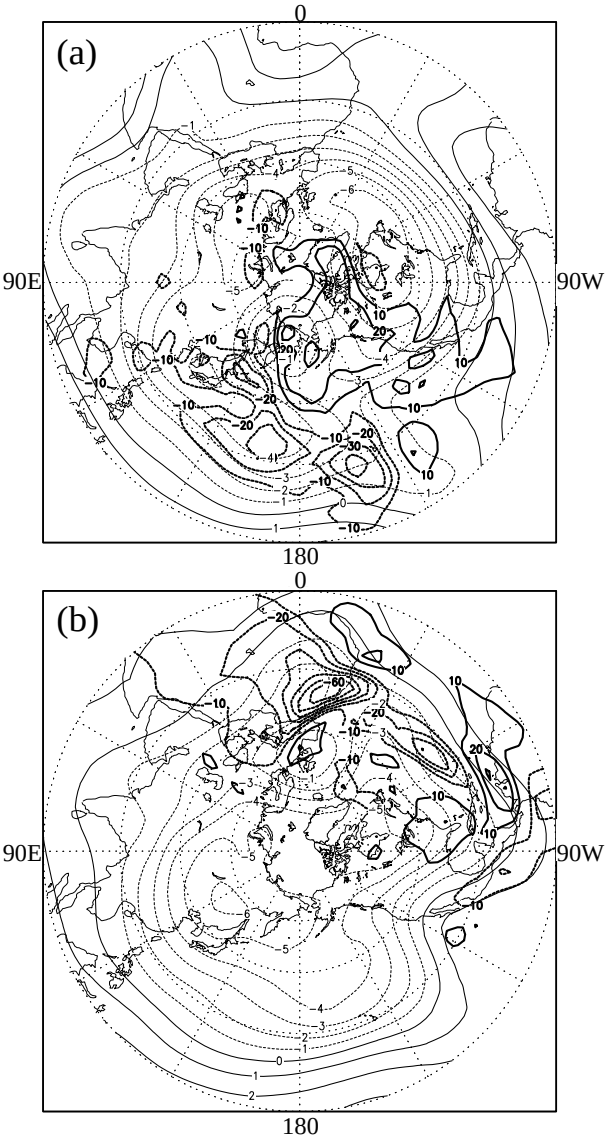

Fig. 5. Same as Fig. 3, except for the gradient (thick line) of the cost function with respect to the initial vorticity forcing. The contours are in increments of 10^{22} m^4. The time mean analysis streamfunctions (thin line) in the corresponding time window are plotted as background by contours in increments of 10^7 m^2 s^{-1} for each case.

4.2 *Minimization of the cost function*

The sensitivity distributions shown in section 4.1 provide the possible locations of the initial vorticity forcing to form blocking. However, due to the constraint of the barotropic vorticity advection over the global domain, only using the sensitivity distribution at $\boldsymbol{f}_c = 0$ is not sufficient to derive the distribution of the initial vorticity forcing. In this section, an iterative optimization procedure using the limited-memory quasi-Newton method (Liu and Nocedal, 1989) is employed to solve for the optimal initial vorticity forcing for each case.

In the minimization procedure, each iteration includes a nonlinear GBS model run (evaluating J), an adjoint model run (evaluating $\nabla_{\boldsymbol{f}_c} J$) and an optimization search process. Starting from $\boldsymbol{f}_c = 0$, (iteration 0), the decreases of the cost function (J, thick-solid line) and the norm of the gradient ($\| \nabla_{\boldsymbol{f}_c} J \|$, solid line) and RMSE (dashed line) over the 48-h time window with the iteration number are displayed in Fig. 6 for Case 1 (panel a) and Case 2 (panel b). In about 10 to 12 iterations, for both cases the cost functions decrease by 95%, and the norm of the gradient is reduced by two orders and the RMSE is reduced by one order. Then, due to the constraint of the global vorticity advection, the norm of the gradient and RMSE stay at the same order level (they decrease very little as the iteration proceeds).

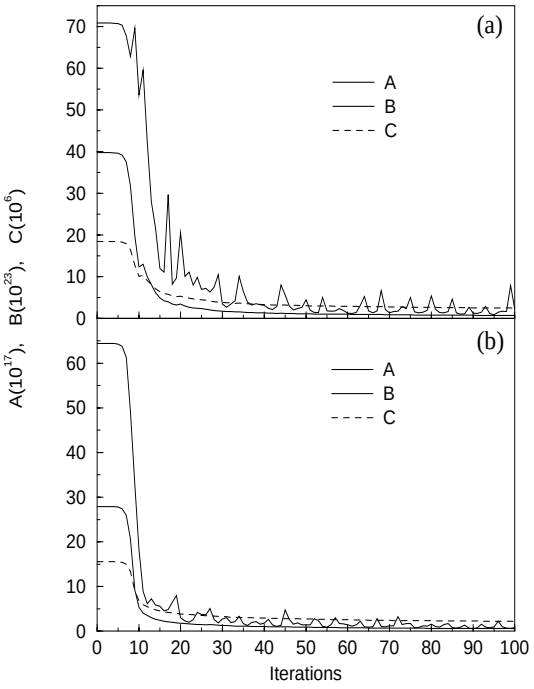

Fig. 6. Changes of the cost function (line A, thick line), the norm of the gradient of the cost function with respect to the initial vorticity forcing (line B, thin line) and the root mean square error (RMSE) (line C, dotted line) with iteration number in the minimization using the streamfunctions at (a) 0000 UTC 28 December 1990 and (b) 0000 UTC 1 November 1980 as initial conditions.

4.3 *Optimal initial vorticity forcings*

The optimal initial vorticity forcing solved from the optimization iterative procedure described in section

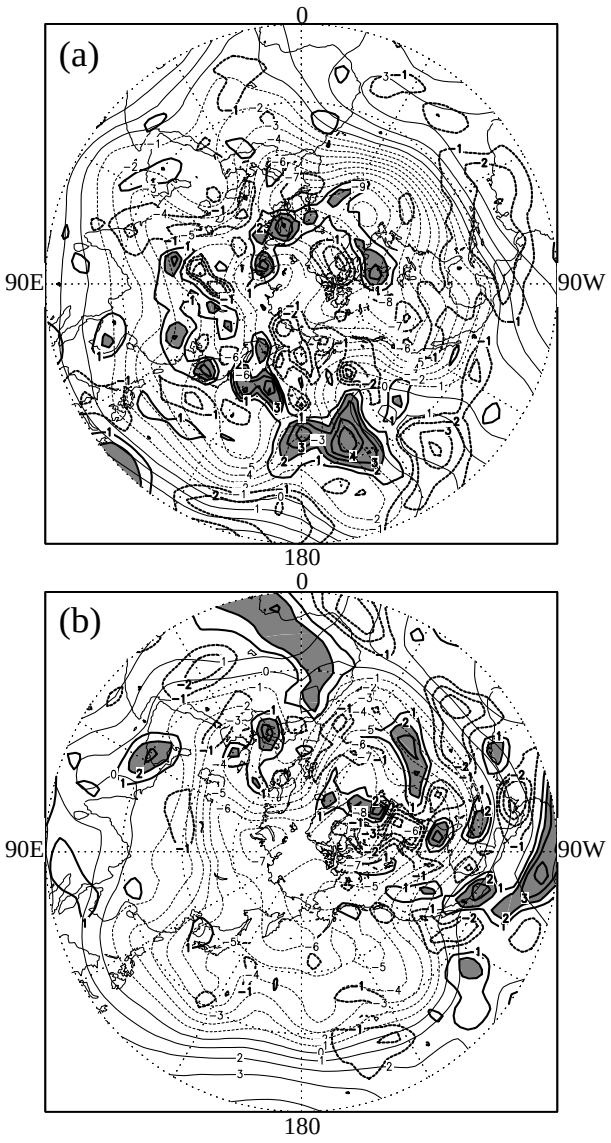

Fig. 7. Same as Fig. 3, except for the optimal initial vorticity forcing (thick line). The contours are in increments of 10^5 s^{-2} and the shading represents areas with values greater than 2×10^5 s^{-2}. The initial streamfunctions at (a) 0000 UTC 28 December 1990 and (b) 0000 UTC 1 November 1980 are plotted by contours in increments of 10^7 m^2 s^{-1} as background.

4.2 is shown in Fig. 7. Panel a and panel b respectively display the distributions of the optimal initial vorticity forcing $\boldsymbol{f}_{\mathrm{opt,c}}$ for Case 1 and Case 2. The initial streamfunctions (0000 UTC 28 December 1990 for Case 1 and 0000 UTC 1 November 1980 for Case 2) are plotted as the background in both panels. Comparing Fig. 7 with Fig. 5, we find that the distributions of the positive/negative $\boldsymbol{f}_{\mathrm{opt,\,c}}$ (Fig. 7) are overall similar to the sensitivity distributions (Fig. 5) with opposite phases. This is consistent with the analyses in section 4.1, i.e., again the gradient (sensitivity) $\| \nabla_{\boldsymbol{f}_{\mathrm{c}}} J \|$ shown in Fig. 5 is evaluated as $\boldsymbol{f}_{\mathrm{c}} = 0$. This phenomenon suggests that if an appropriate scalar is chosen, to some accuracy, the opposite phase of the gradient may serve as an approximation of the vorticity forcing.

In the dynamics of barotropic vorticity advection, the derived initial vorticity forcing serves as a synoptic-scale disturbance on the planetary trough/ridge motions. Figure 7 indicates that for both cases the negative (anticyclonic vortex) initial vorticity forcing is distributed over the blocking high region and the positive (cyclonic vortex) initial vorticity forcing is distributed along the upstream low troughs. Over the downstream low troughs in both cases, the central regions are the positive (cyclonic vortex) initial vorticity forcing. Those cyclonic/anticyclonic vorticity sources favor the development of the anticyclonic vortex over the blocking high and the cyclonic vortex at its upstream/downstream side. However, for the dipole pattern blocking (Case 2), a big cyclonic vorticity forcing center distributes over the cut-off low center and its southeast region (the trough bottom) while for the "Ω" block pattern (Case 1) at the trough bottom is weak anticyclonic vorticity forcing. This is consistent with the requirement of a stronger cyclonic vorticity advection to form a cut-off low center over the south of the blocking high for this blocking pattern.

In addition, it seems that the location of the greatest positive vorticity forcing center for Case 1 falls in the region described by Colucci and Alberta (1996) (panel a in Fig. 7), i.e., $v' > 0, u' < 0$, and $v/u > 0.5$. For both cases, a few large vorticity forcing centers are located over the tropics/subtropics. Since the derived vorticity forcing includes all factors that the dynamics of the barotropic vorticity advection fails to describe, such as baroclinic disturbance, vertical advection, etc., physically interpreting the derived vorticity forcing centers requires further study, including the use of more complex models.

In the next section, we will show that using these derived vorticity forcings as the initial 24-h synoptic-scale perturbations on the initial streamfunction fields (0000 UTC 28 December 1990 for Case 1 and 0000 UTC 1 November 1980 for Case 2), the barotropic nonlinear advection process can reconstruct the onset of these blocking processes.

5. Impact of the optimal initial vorticity forcing on blocking simulation and forecasts

5.1 *Reconstruction of the blocking onset processes*

Using the derived optimal initial vorticity forcing (thick lines) shown in Fig. 7, we run the barotropic model again (the initial conditions are the same as before) and make 10-day forecasts for both cases (the forecasts with/without the optimal initial vorticity forcing are called the optimal/control forecasts, hereafter). The first 5-day control (left column) and optimal (right column) forecasts for Case 1 and Case 2 are exhibited in Fig. 8 and Fig. 9, respectively. Comparing these forecasts with the corresponding analyses in Fig. 1 (Case 1) and Fig. 2 (Case 2), it is observed that for both cases the introduction of the optimal initial vorticity forcing mostly reconstructs the process of the block onset while the control forecasts entirely lose the capability to describe the strengthening ridge which develops into a blocking high (for both cases), and/or a deepening trough which develops into a cut-off low center at the right phase (for Case 2).

The reconstruction of the block onset above using the derived initial vorticity forcing tells us that the formation of blocking can be mostly described by a barotropic nonlinear advection process. In the process, the wave- (synoptic-scale) flow (planetary-scale) interaction plays a very important role. On a favorite planetary-scale flow, a certain synoptic-scale disturbance can cause the block onset by the interaction of the synoptic-planetary scales.

5.2 *Improvement of blocking forecasts*

In order to examine the impact of the optimal initial vorticity forcing on the forecast of the blocking events by the barotropic model, both control and optimal forecasts are extended up to 10 days. Figure 10 presents the daily evolution of Case 1 (left panels) and Case 2 (right panels) forecasts from day 6 to day 10. From the figure, it is observed that for Case 1 with the optimal initial vorticity forcing, the phase of the forecasted blocking high (high ridge) over the Bering Sea is traceable for 10 days although the phase is lagged to the analysis from day 6 on, and the trough over the west of North America is greatly exaggerated. For Case 2, although the trough of optimal forecasts over the northern Atlantic is exaggerated, the blocking high over the western North Atlantic is traceable up to 8

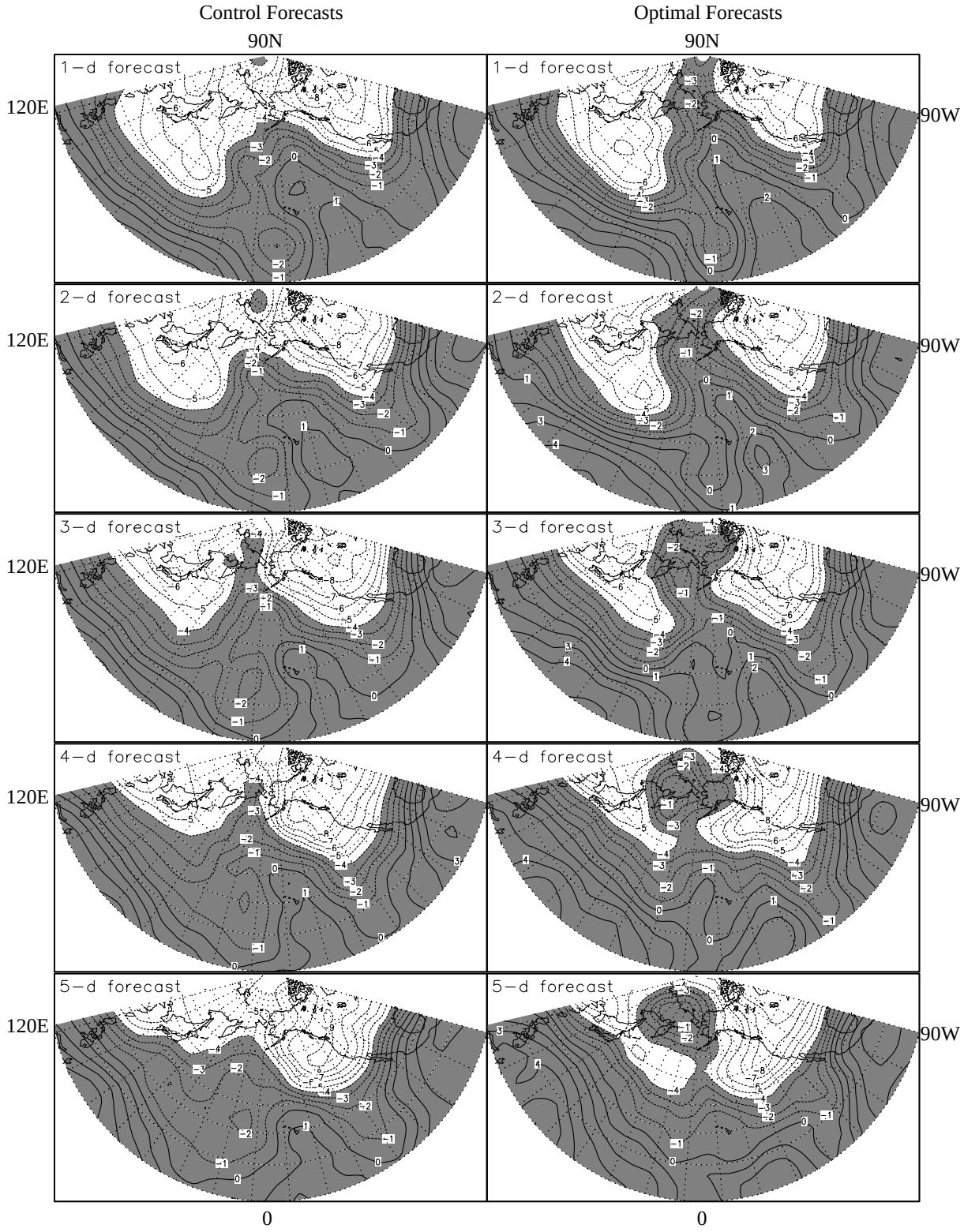

Fig. 8. Daily sequences of the streamfunctions of control forecasts (without the initial vorticity forcing) (left) and optimal forecasts (with the optimal initial vorticity forcing) (right) using the analysis streamfunction at 0000 UTC 28 December 1990 as initial conditions, from day 1 to day 5, over the domain of 0°–90°N, 120°–270°E. The contours are in increments of 10^7 m^2 s^{-1}. The shading represents areas with values greater than -4×10^7 m^2 s^{-1}.

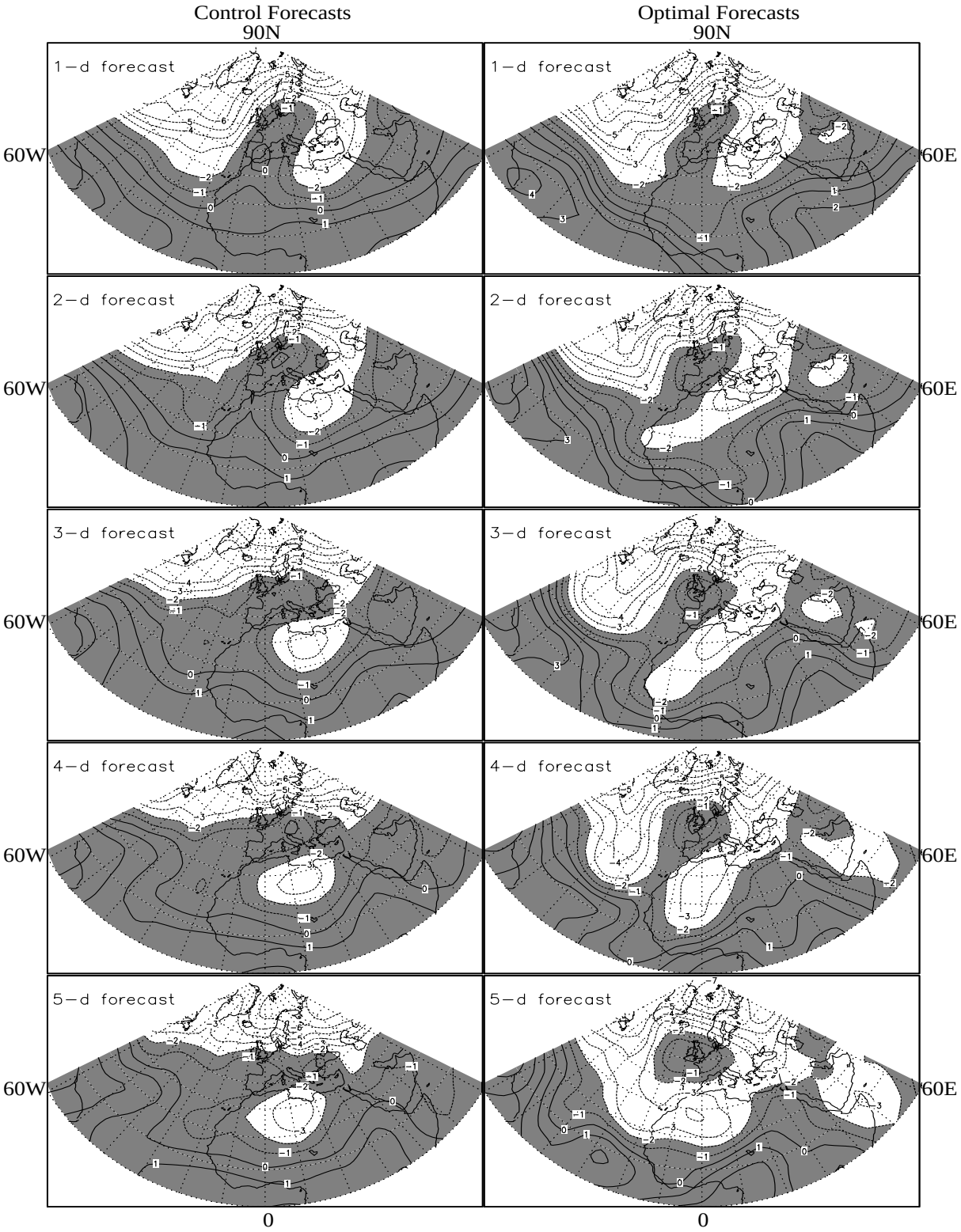

Fig. 9. Same as Fig. 8, except using the analysis at 0000 UTC 1 November 1980 as initial conditions, over the domain of 0°–90°N, 60°W–60°E. The shading represents areas with values greater than -2×10^7 m^2 s^{-1}.

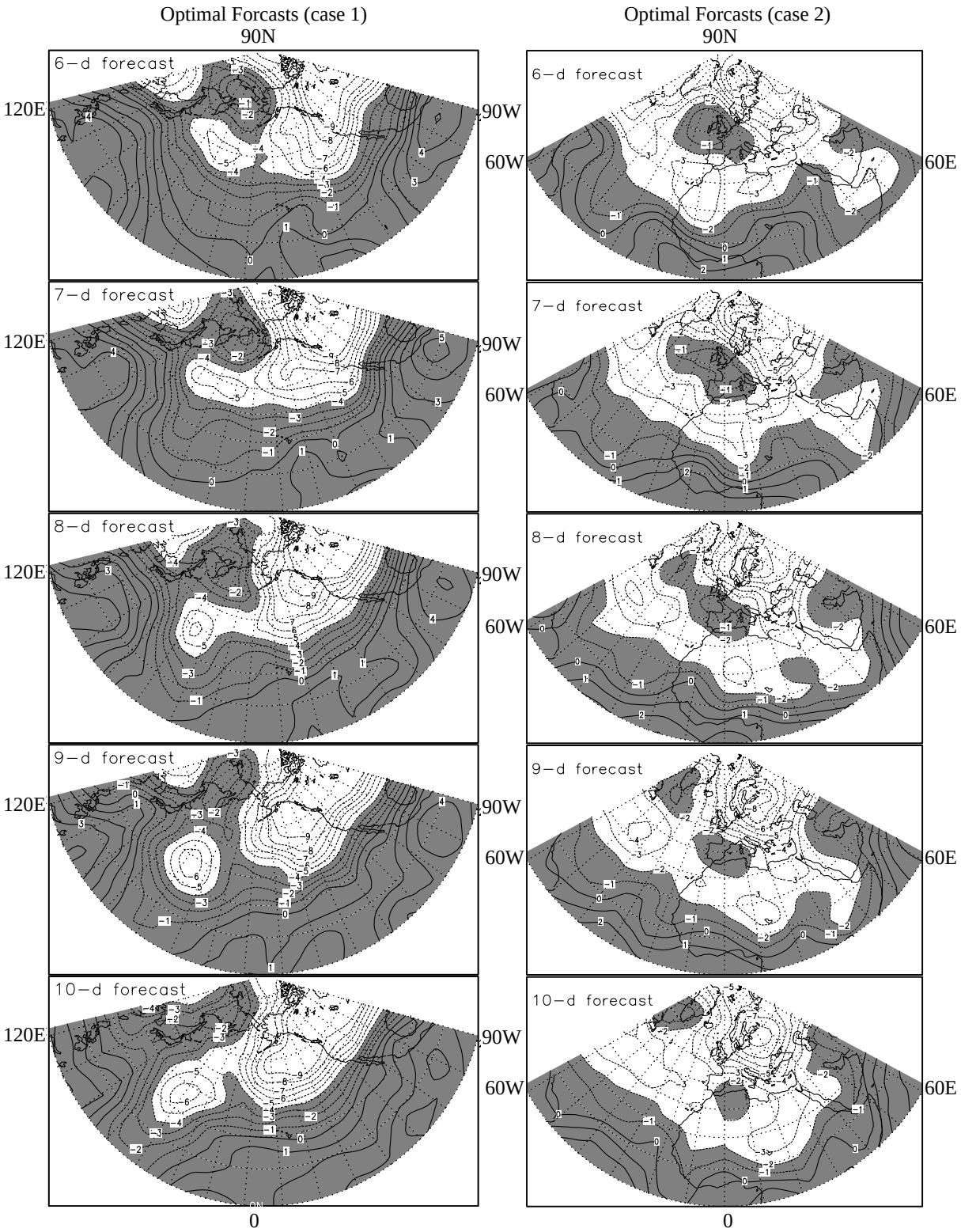

Fig. 10. Same as Fig. 8, except the optimal forecasts are from day 6 to day 10 using the analysis streamfunctions at 0000 UTC 28 December 1990 over the domain of 0°–90°N, 120°–270°E (left) and 0000 UTC 1 November 1980 over the domain of 0°–90°N, 60°W–60°E (right) as initial conditions. The shading represents areas with values greater than -4×10^7 m^2 s^{-1} (left) and -2×10^7 m^2 s^{-1} (right).

days. Of course, the control forecasts do not have any traceable ridge or trough during the whole period. These results show that although the barotropic vorticity advection dynamics is only an approximate description (probably leading order), rather than a complete picture of the complex blocking mechanism (baroclinic processes, for instance), the optimal vorticity forcings derived from a 4D variational approach have a certain capability to improve forecasts. The optimization process in the 4D variational approach accounts for all unresolved processes by the simplified dynamics as the vorticity forcing term, so as to simplify the complexity, to some degree. Once the optimal vorticity forcings for blocking onset/development are derived, the forced barotropic vorticity model is able to extend the valid forecasts.

6. Summary and discussions

With the aid of a global barotropic model, the role of the interaction of synoptic-scale disturbances and planetary flows in block onset is examined by a 4D variational approach in this study. A cost function is defined to measure the squared errors of the forecasted streamfunctions during the block onset period over a selected blocking domain. The sensitivity of the block onset with respect to the initial synoptic-scale disturbance is studied by examining the gradient of the defined cost function with respect to the initial (the first 24 hours, in this study) vorticity forcing, which is evaluated by the adjoint integration. The distribution of the sensitivity superposed on the initial streamfunction tells us the possible need of the synoptic disturbance over a appropriate planetary flow for the block onset. Furthermore, connecting the evaluation of the defined cost function and the gradients with the limited-memory quasi-Newton optimization algorithm (Liu and Nocedal, 1989) the optimal initial vorticity forcing for the block onset is solved by an iterative minimization procedure.

For two studied cases, the introduction of the optimal initial vorticity forcing into the nonlinear barotropic vorticity advection process mostly reconstructs the process of the block onset. This phenomenon tells us that although the onset and development of blocks is a rather complex process with many factors involved, the nonlinear barotropic vorticity advection process can be treated as the leading order approximation. In the process, the (synoptic-scale) wave-flow (planetary-scale) interaction plays a very important role. On an appropriate planetary-scale flow, a certain synoptic-scale disturbance can cause the block onset by the interaction of the synoptic-planetary scales. The extended forecasts up to 10 days show that the introduction of the optimal initial vorticity forcings derived from the 4D variational approach can extend the valid forecasts 2 to 3 days in this simple model study case.

The experimental results in this study show that the 4D variational approach has a good potential to be applied to study the dynamics of medium-range weather processes. However, under the framework of the barotropic vorticity advection, the derived vorticity forcing blends all factors that the dynamics of the barotropic vorticity advection leaves unresolved. It is very difficult to connect the derived forcing distribution with the real atmospheric forcing distribution due to the model bias. This simple model case is only an initial trial. Applying the framework in this study to a complex model will further our understanding of the mechanism of the atmospheric/oceanic processes and improve their forecasting.

In addition, it is worth mentioning that the derived results through this 4D variational approach may have some dependency on the definition of the cost function (Frederiksen, 2000). This study only uses a sum of squared forecasting errors of the streamfunctions as a distance measurement of the model simulation and "observations". In the future, a thorugh examination of the dependency of the derived optimal vorticity forcing on the definition of the cost function needs to be done for further application of this approach.

Acknowledgments. The initial codes of the forward barotropic model were provided by Dr. Jon E. Ahlquist. The authors would like to further thank Jon E. Dr. Ahlquist for his generous discussions and suggestions during this study. We also wish to thank Dr. H. Wang for her comments on earlier versions of this manuscript. Thanks also go to two anonymous reviewers for thorough and helpful comments and suggestions.

REFERENCES

Berggren, R., B. Bolin, and C. G. Rossby, 1949: An aerological study of zonal motion, its perturbation and breakdown. *Tellus*, **1**, 14–37.

Cacuci, D. G., 1981a: Sensitivity theory for nonlinear systems. I: Nonlinear functional analysis approach. *J. Math. Phys.*, **22**, 2794–2802.

Cacuci, D. G., 1981b: Sensitivity theory for nonlinear systems. II: Extensions to additional classes of responses. *J. Math. Phys.*, **22**, 2803–2812.

Cacuci, D. G., 1988: The forward and adjoint methods of sensitivity analysis. *Uncertainty Analysis*, Yigal Ronen, Ed., CRC Press, Inc., 71–144.

Charney, J. G., and J. G. DeVore, 1979: Multiple flow equilibria in the atmosphere and blocking. *J. Atmos. Sci.*, **36**, 1205–1216.

Colucci, S. J., 1985: Explosive cyclogenesis and large-scale circulation changes: Implications for atmospheric blocking. *J. Atmos. Sci.*, **42**, 2701–2717.

Colucci, S. J., 1987: Comparative diagnosis of blocking versus nonblocking planetary-scale circulation changes during synoptic-scale cyclogensis. *J. Atmos. Sci.*, **44**, 124–139.

Colucci, S. J., and T. L. Alberta, 1996: Planetary-scale climatology of explosive cyclogensis and blocking. *Mon. Wea. Rev.*, **124**, 2509–2520.

Dole, R. M., 1989: Life cycles of persistent anomalies. Part I: Evolution of 500 mb height fields. *Mon. Wea. Rev.*, **117**, 177–211.

Dole, R. M., and N. D. Gordon, 1983: Persistent anomalies of the extra-tropical Northern Hemisphere wintertime circulation: Geographical distribution and regional persistence characteristics. *Mon. Wea. Rev.*, **111**, 1567–1586.

Frederiksen, J. S., 1982: A unified three-dimensional instability theory of the onset of blocking and cyclogenesis. *J. Atmos. Sci.*, **39**, 969–982.

Frederiksen, J. S., 1989: The role of instability during the onset of blocking and cyclogenesis in Northern Hemisphere synoptic flows. *J. Atmos. Sci.*, **46**, 1076–1092.

Frederiksen, J. S., 1998: Precursors to blocking anomalies: The tangent linear and inverse problem. *J. Atmos. Sci.*, **55**, 2419–2436.

Frederiksen, J. S., 2000: Singular vectors, finite-time normal modes, and error growth during blocking. *J. Atmos. Sci.*, **57**, 312–333.

Frederiksen, J. S., and R. C. Bell, 1990: North Atlantic blocking during January 1979: Linear theory. *Quart. J. Roy. Meteor. Soc.*, **116**, 1289–1313.

Haltiner, G. J., and R. T. Williams, 1980: *Numerical Prediction and Dynamic Meteorology.* 2nd ed., Wiley and Sons, 477pp.

LeDimet, F. X., and O. Talagrand, 1986: Variational algorithms for analysis and assimilation of Meteorological observations: Theoretical aspects. *Tellus.*, **38A**, 97–110.

Li, Z., A. Barcilon, and I. M. Navon, 1999: Study of block onset using sensitivity perturbation in climatological flows. *Mon. Wea. Rev.*, **127**, 879–900.

Liu, D. C., and J. Nocedal, 1989: On the limited memory BFGS method for large scale optimization. *Mathematical Programming*, **45**, 503–528.

Lupo, A. R., and P. J. Smith, 1995: Climatological features of blocking anticyclones in the Northern Hemisphere. *Tellus*, **47**, 439–456.

Nakamura, H., and J. M. Wallace, 1990: Observed changes in the baroclinic wave activity during the life cycles of low-frequency circulation anomalies. *J. Atmos. Sci.*, **47**, 1100–1116.

Namias, J., 1964: Seasonal persistence and the recurrence of European blocking during 1958–60. *Tellus*, **16**, 394–407.

Navon, I. M., X. Zou, J. Derber, and J. Sela, 1992: Variational data assimilation with an adiabatic version of the NMC spectral model. *Mon. Wea. Rev.*, **120**, 1433–1446.

Pondeca, M. S. F. V, A. Barcilon, and X. Zou, 1998: An adjoint sensitivity study of the efficacy of modal and nonmodal perturbations in causing model block onset. *J. Atmos. Sci.*, **55**, 2095–2118.

Reinhold, B. P., and R. J. Pierrehumbert, 1982: Dynamics of weather regimes: Quasi-stationary waves and blocking. *Mon. Wea. Rev.*, **110**, 1105–1145.

Rex, D. F., 1950: Blocking action in the middle troposphere and its effect upon regional climate. II: The climatology of blocking action. *Tellus*, **2**, 275–301.

Sanders, F., and J. Gyakum, 1980: The synoptic-dynamic climatology of the bomb. *Mon. Wea. Rev.*, **108**, 1589–1606.

Shutts, G. J., 1983: The propogation of eddies in diffluent jet streams: Eddy forcing of "blocking" flows fields. *Quart. J. Roy. Meteor. Soc.*, **109**, 737–762.

Sirkes, Z., and E. Tziperman, 1997: Finite difference of adjoint or adjoint of finite difference. *Mon. Wea. Rev.*, **125**, 3373–3378.

Tibaldi, S., and A. Buzzi, 1983: Effects of orography on Mediterranean lee cyclogenesis and its relationship to European blocking. *Tellus*, **35A**, 269–286.

Tsou, C. H., and P. J. Smith, 1990: The role of synoptic/planetary-scale interactions during the development of a blocking anticyclone. *Tellus*, **42A**, 174–193.

Tung, K. K., and R. S. Lindzen, 1979: A theory of stationary long waves. Part I: A simple theory of blocking. *Mon. Wea. Rev.*, **107**, 714–734.

Zhang, S., X. Zhou and J. E. Ahlquist, 2001: Examination of numerical results from tangent linear and adjoint of discontinuous nonlinear models. *Mon. Wea. Rev*, **129**, 2791–2804.

Zou, X., A. Barcilon, I. M. Navon, J. Whitaker, and D. G. Cacuci, 1993: An adjoint sensitivity study of blocking in a two-layer isentropic model. *Mon. Wea. Rev.*, **121**, 2833–2857.